Graphene with Patterned Fluorination: Morphology Modulation and Implications

Haifei Zhan[1], Guiyong Zhang[2], John M. Bell[1], and Yuantong Gu[1,]*

[1]School of Chemistry, Physics and Mechanical Engineering, Queensland University of Technology (QUT), 2 George St, Brisbane QLD 4001, Australia

[2]State Key laboratory of Structural Analysis for Industrial Equipment, School of Naval Architecture, Dalian University of Technology, Dalian 116024, China

***Corresponding Author:** Prof. Yuantong Gu

Mailing Address: School of Chemistry, Physics and Mechanical Engineering,
Queensland University of Technology (QUT),
GPO Box 2434, Brisbane, QLD 4001, Australia

Telephones: +61-7-31381009 **Fax:** +61-7-31381469

E-mail: yuantong.gu@qut.edu.au

ABSTRACT: Recent years' have witnessed a large volume of works on the modification of graphene, however an understanding of the associated morphology or mechanical properties changes is still lacking, which is vital for its engineering implementation. By taking the C_4F fluorination as an example, we find that the morphology of both graphene sheet (GS) and graphene nanoribbon (GNR) can be effectively tailored by fluorination patterning, via molecular dynamics simulations. The fluorine atom produces out-of-plane forces which trigger several intriguing morphology changes to monolayer graphene, including zigzag, folded, ruffle, nanoscroll and chain structures. Notably, for multi-layer GNR, the delamination and climbing phenomena of the surface layer are observed. Further studies show that the fluorination pattern can also be utilized to modulate the mechanical properties of graphene, e.g., about 40% increase of the effective yield strain is observed for the examined GNR with fluorination patterns. This study not only demonstrates the significant impacts on the morphology of graphene from fluorination, but also suggests an effective avenue to tailor the morphology and thus mechanical properties of GS and GNR.

KEYWORDS: fluorination, graphene, morphology, nanoscroll, mechanical property

1. INTRODUCTION

The exceptional physical, chemical, electrical and mechanical properties of graphene make it as an appealing building block for wide applications, such as fuel cells, sensors, flexible electronics, and supercapacitors.[1] Owing to its strong sp^2 bonds and low mass density, graphene possesses superior thermal transport properties and electrical conductivity.[2-3] For instance, graphene is reported to possess a thermal conductivity exceeding ~3,000 W/mK,[4] a mobility as high as 200,000 $cm^2V^{-1}s^{-1}$ at low temperatures, and it is alos reported to demonstrate the quantum Hall effect at room temperature.[5] Together with the high theoretical

surface-to-mass ratio[6] (~2,600 m^2/g), superior Young's modulus (as high as 1 TPa)[7] and chemical stability, graphene shows great potential to address the ever growing demand for portable and wearable energy conversion and storage devices.[8]

To facilitate different applications, graphene usually requires certain modifications. For instance, for biomedicine applications, graphene needs to be oxidised or functionalized to avoid or suppress cytotoxicity and enhance its biocompatibility.[9] In thermal management applications, some electronic devices demand a high thermal conductivity to ensure stability (e.g., circuits, interconnects and transistors), while thermoelectric devices desire a strongly suppressed thermal conductivity to ensure its high efficiency.[10] More importantly, pristine graphene is intrinsically gapless which greatly impedes its integration into electronic devices. In this regard, various approaches have been developed to tailor the properties of graphene, such as doping (e.g., Au[11] and N[12]), covalent and non-covalent functionalization[13-14] (e.g., hydrogen[15] or methyl[16] functionalization), and defects engineering (e.g., grain boundary and nano-holes).[17-18] Researchers have reported the successful synthesisation of graphene with various functional groups (such as hydroxyl, epoxy and carbonyl)[19] and doping elements (e.g., N, B, H).[12, 20] Among these graphene derivatives, fluorinated graphene has received the most intensive interests owing to the strong electronegativity and superhydrophobicity of the covalently bonded F, and because of its doping-ratio-dependent band gap.[21-22]

To date, two general strategies have been developed to produce fluorinated graphene, directly fluorinating graphene sheets (GSs) and exfoliating from graphite fluoride.[23] Both theoretical and experimental studies have reported that several stable C_nF structures exist, such as the full fluorination CF,[24] C_4F and C_2F structures.[25] By using graphene oxide and liquid diethylaminosulfur trifluoride as starting materials, researchers proposed a facile solution to prepare fluorinated graphene with tailorable fluorine content.[21] Specifically, it has been reported that graphene with different fluorination contents possess different electronic

and magnetic properties,[26-27] and that the control of nanopatterning of fluorinated graphene can selectively reduce insulating fluorinated graphene to conducting and semiconducting graphene.[28] The availability of controllable fluorination on graphene through either electron beam irradiation[28] or thermochemical nanolithography[29] opens up an avenue to control its structure, which is vital for its high-end applications (e.g., electronics and photonics).[30] However, a comprehensive understanding of how different fluorination patterns might influence the structure or morphology of graphene is still lacking. In this paper, based upon molecular dynamics (MD) simulations and theoretical analysis, we find that the morphology of either graphene sheets or graphene nanoribbons can be effectively tailored through fluorination patterning. This study provides valuable guidelines for the integration and fabrication of fluorinated graphene-based devices.

2. METHODS

The morphology changes of the fluorinated graphene were tracked through a series of MD simulations. Emphasizes were put on free-standing GS or GNR models, i.e., no extra constrain or substrate was considered. The recently developed reactive force field (ReaxFF) potential has been adopted to describe the interaction between C and F atoms, which predicts comparable mechanical properties of graphene or hydrogenated graphene with that obtained from the commonly used AIREBO potential.[31] The ReaxFF force field is a general bond-order-dependent potential that utilizes a relationship between bond distance and bond order.[32] It contains both many-body bonded and non-bonded interactions (i.e., Coulomb and van der Waals interaction), which can describe bond formation and dissociation. The applied ReaxFF potential has been shown to well reproduce key quantum mechanical and thermal properties of relevant carbon-fluorine cluster systems, such as $H_3C\text{-}CF_2\text{-}CH_3$, $H_3C\text{-}CF(CH_3)\text{-}CH_3$, and F_2.[31]

The initial fluorinated graphene model was established based on recent first principle calculations.[25] For the graphene nanoribbon (GNR) model, a periodic boundary condition was applied along the length direction with a free boundary condition along the width direction. For the graphene sheet (GS) model, periodic boundary conditions were applied along both lateral directions. The conjugate gradient minimization method was firstly applied to the initial model to obtain the equilibrium configuration of the sample. Afterwards, the sample was equilibrated using a Nose-Hoover thermostat[33-34] under ambient conditions (temperature = 300 K and pressure = 1 atm). Such equilibrium procedure was continued for more than 150 ps to ensure a stable structure was achieved.

Additionally, tensile deformation was conducted to further understand how morphology changes will affect the mechanical properties of the GNR. For this purpose two GNR models were compared: a pristine GNR (initial size of ~ 4 × 25.5 nm) and its counterpart with an almost evenly distributed fluorination pattern (Figure 7a). A constant strain rate (10^{-6} fs^{-1}) was applied after the relaxation of both models. During the tensile loading the structure was allowed a 1000 fs relaxation following each 0.002 strain increment to ensure a uniform tensile deformation. To reduce the thermal fluctuations influence, the temperature was kept at 5 K during the simulation. Due to the presence of sp^3 bonds, a small time step of 0.1 fs was used and all simulations were performed using the software package *LAMMPS*.[35]

3. RESULTS AND DISCUSSIONS

3.1 Graphene Sheet

Initially, we looked at how different fluorination patterns influence the morphology of monolayer GS. We focused on one of the stable C_nF structures, ($-C_4F$) with either one-side or double-side doping, as illustrated in Figure 1b and 1c (such fluorination patterns on graphene have been reported experimentally[27]). Considering the periodic boundary conditions, the two

fluorination patterns are evenly distributed along the length direction of the GS (Figure 1b). Here, the armchair direction is denoted as the length direction and the corresponding vertical zigzag direction is the width direction. For discussion convenience, the doping ratio is defined as the ratio of fluorination length W to the period length L, i.e., $_F = W / L$. Here L is half of the total sample length (L_{tot}). To identify the potential morphology changes, sample lengths ranging from ~ 6.8 to ~ 27.2 nm have been considered, corresponding to five groups of GS samples. A uniform width of ~ 2.4 nm has been considered for all examined GSs, and the doping ratio from 0 ~ 1 have been tested in each group. We note that a small width (~ 2.4 nm) is adopted in order to reduce the computational cost, and it will not influence the simulation results due to the periodic boundary conditions.

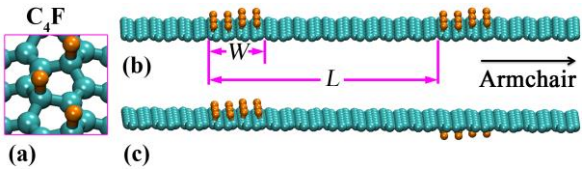

Figure 1. (a) The stable C_4F structure; schematic views of the: (b) single-side fluorination pattern, and (c) double-side fluorination pattern. F and C atoms are coloured as orange and cyan, respectively.

In general, the morphology of GS is observed to rely heavily on the width of the fluorination pattern. The existence of C_4F is found to induce out-of-plane forces, which lead to the local out-of-plane deformation. Specifically, for a small L, the patterned single-side fluorination will drive the GS to deform into a wave shape (Figure 2a), where the wave amplitude differs for different fluorination ratios. While for larger L, the GS is observed to transit from a wave shape to a ruffle structure at medium doping ratio (Figure 2b) and resume the wave shape at high doping ratio. When the C_4F fluorination covers the whole domain, the GS becomes flat again.

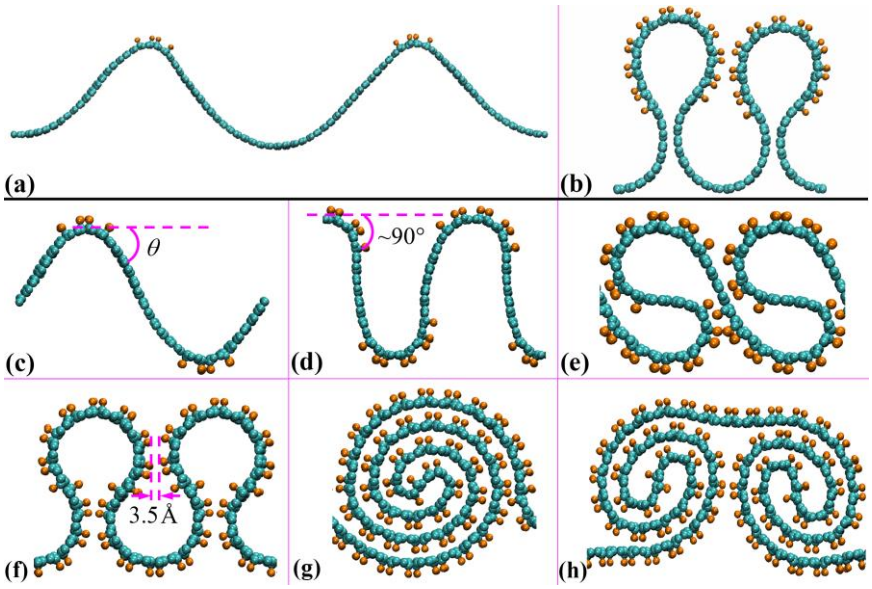

Figure 2. Morphology changes of GS (width of about 2.4 nm) resulted from the patterned fluorination with different doping ratios η_F. GS with single-side fluorination pattern: (a) wave shape and (b) ruffle shape; GS with double-side fluorination pattern: (c) zigzag structure, (d) zigzag structure, (e) folded shape, (f) ruffle structure, (g) nanoscroll structure, and (h) chain structure. Note that for illustration purpose, the presented atomic configurations contain their periodic images in the length direction.

In comparison, the double-sided C_4F induces a more complex structural change, including the formations of zigzag, folded, ruffle, nanoscroll, and chain structures. As illustrated in Figure 2c, the GS deforms into a zigzag shape at low doping ratio, which contains symmetrically bent fluorinated regions and planar undoped graphene regions. The increase of the fluorination pattern width gradually increases the bent angle to 90° as shown in Figure 2d, similar as reported for graphene with hydrogenation pattern.[36] Further increase of the doping ratio is observed to lead to a folded structure (Figure 2e), in which the inter-layer long-range interactions (i.e., van der Waal forces) between graphene segments start to play a role. With increasing pattern width *W*, more interesting morphology changes are observed. As seen in Figure 2f, the fully double-side C_4F fluorinated GS (stripe length *L* of

6.8 nm) is found to deform into a ruffle morphology, similar to the case with single-side fluorination (Figure 2b). Notably, when the fluorination pattern width is larger than ~ 2 nm and the doping ratio η_F > ~ 0.6, the GS can roll up into a nanoscroll structure (Figure 2g) or chain structure (Figure 2h). Further simulations reveal that other stable C_nF fluorination pattern ($n>1$), i.e., C_2F boat structure, also result in similar morphology changes (see Supporting Information, S1). A recent experimental work has reported the atomically resolved imaging of such highly ordered single side C_2F fluorination on graphene.[37]

To unveil the mechanisms that determine the different morphologies, we calculated the force distribution in the fluorinated region. A super cell of 3.68 × 10.64 $Å^2$ (with W = 8.51 Å) is chosen to plot the force distribution as illustrated in the middle of Figure 3a. Each solid circle represents two carbon atoms along the width of the super cell, and each open circle denotes one fluorine atom bonded to the neighboring carbon atom. Evidently, the C_4F fluorination induces a relatively large out-of-plane force, with a maximum force around 34 eV/Å. Considering the symmetry of the deformation and the periodic boundary conditions, half of the fluorination region can be simplified as a cantilever beam subjected to several concentrated constant forces from the fixed end of the beam (upper of Figure 3b). These forces have induced a net bending moment M around 0.9 eV at a distance of $W/2$ from the fixed end of the beam (lower of Figure 3b). According to the classical beam theory, the bending angle θ is related to the bending moment M by $\theta = MW / 2EI$, where EI is the bending rigidity. In other words, θ is a linear function of the fluorination pattern width and independent of the beam length L. Such conclusion is consistent with the simulations for another four groups of fluorinated GSs with their length ranging from 3.40 ~ 8.51 nm, from which an approximately linear relation between θ and W is found as plotted in Figure 3c. We should notice that larger stripe length L will increase the instability of the structure, which will make the GS vulnerable to deform into a folded shape rather than a regular zigzag shape

even when the bending angle is still below 90° (or the pattern width *W*/2 is smaller than around 17 Å). In other words, GS with large strip length will show local folded structure, though the local bending angle between the doped and undoped region still follows the linear relation.

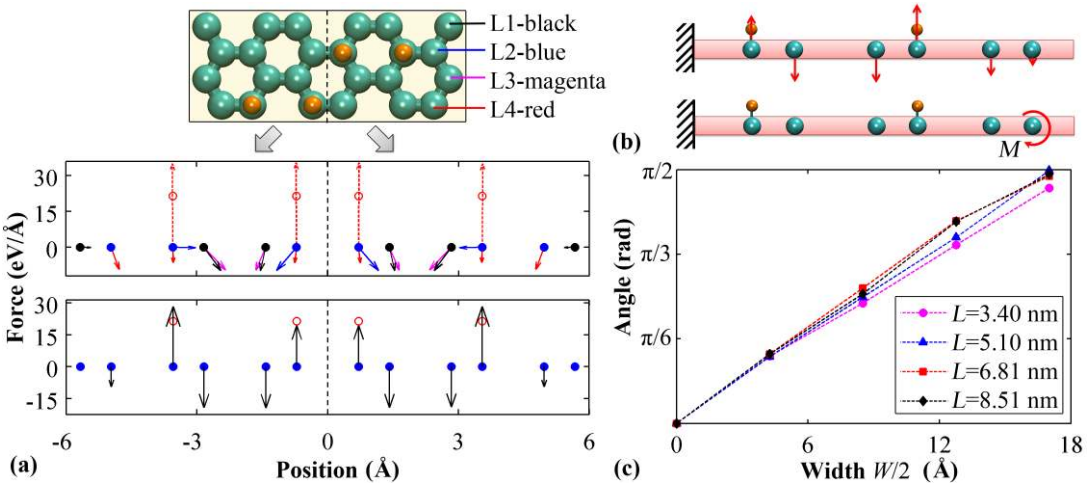

Figure 3. (a) Upper shows a super cell graphene with C_4F fluorination. Middle is the corresponding force distribution in each carbon atom (black, blue, magenta and red represent the atomic force in rows from L1~L4, respectively). Bottom is the out-of-plane net force per unit width. The arrows represent the force acting on each of the C atoms, with the dashed arrows denoting the force induced by the F atoms. (b) A cantilever beam model for the C_4F fluorinated graphene. (c) The bending angle as a function of the width (*W*/2) of the C_4F fluorination pattern.

Additionally, according to Figure 3a, the force is distributed symmetrically and equally in both lateral directions. In other words, the morphology changes of GS will also be triggered while the fluorination pattern is along the zigzag direction, which is verified from our further simulations as presented in the Supporting Information (S2). It is concluded that the morphologies of GSs can be effectively controlled through the modulation of the fluorination pattern. It should be noted that although rare experimental studies have been reported so far for the morphology modulation of graphene using surface fluorine

modification, the morphology control through patterned hydrogenation has been widely discussed for graphene[36, 38] and carbon nanotubes.[39] A very recent work has also shown that the single-side fluorination of graphene can greatly enhance friction due to increased corrugation.[40] It is worth mentioning that the thermal vibration should also influence the observed morphology change. Current work has emphasized on the ambient temperature (300 K) and a similar morphology change phenomenon is expected to occur in a wide range of temperature. However, further studies are still deserved to identify when the morphology change will be insignificant due to the increased thermal vibration at high temperature.

3.2 Graphene Nanoribbon

In engineering applications, such as digital applications, graphene is usually utilized as graphene nanoribbon (GNR) to open a bandgap.[41] In this section, we examine how the morphology of the GNR can be changed through pattern fluorination. Two groups of samples have been established with the GNRs either armchair-edged or zigzag-edged. In each group, we consider the single-side or double-side fluorination patterns that are either parallel or perpendicular to the length direction of the nanoribbon (see Supporting Information for model configurations). For discussion consistency, an identical size has been chosen for all samples, i.e., ~ 6×6 nm^2, and the doping ratio from 0 to 1 is examined. It is found that for all tested GNRs, a double-side fluorination will lead to a similar morphology change. That is the structure deforms uniformly along the pattern direction, which leads to the formation of a zigzag shape at low doping ratio and a folded structure for larger fluorination pattern (see Supporting Information, S3).

For the single-side fluorination, the morphology changes preferably happen along the width direction of the nanoribbon. Figures 4a to 4c illustrate the morphology changes of the armchair-edged GNRs with different percentages of single-side C_4F fluorination parallel to the length direction of the sample. As is seen, at low fluorination ratios, the out-of-plane

forces in the fluorinated regions bend the GNR (Figure 4a). With increasing fluorination pattern width, the GNR is found to roll into a nanoscroll structure (Figure 4b), which becomes more evident for higher doping ratio (Figure 4c). For the GNR with fluorination pattern perpendicular to the length direction, a low doping ratio is found to initiate a local buckling along the length direction (Figure 4d, $\eta_F = 43\%$), which is much less evident comparing with its counterpart with parallel fluorination pattern (Figure 4a). However, a higher doping ratio is found to drive the GNR to deformation into a nanoscroll along the width direction (Figure 4e, $\eta_F = 71\%$). Interestingly, for the full C_4F fluorinated case, the GNR is found to change into a semi-nanotube structure rather than a nanoscroll structure (see Figure 4f). Similar morphology change patterns have also been observed for the zigzag-edged GNRs. We should note that the edge stress could also induce significant morphology changes to GS or GNR.[42] While, above estimations have shown that the out-of-plane force (approaching to 34 eV/Å) induced by the fluorination is much larger than that resulted from the edge stress (~ 1.05 and 2.05 eV/Å for armchair- and zigzag-edged graphene, respectively).[42] Together with the periodic boundary conditions and relatively large sample width (for GNR) being applied, the edge stress is supposed to have ignorable influence to the current discussion.

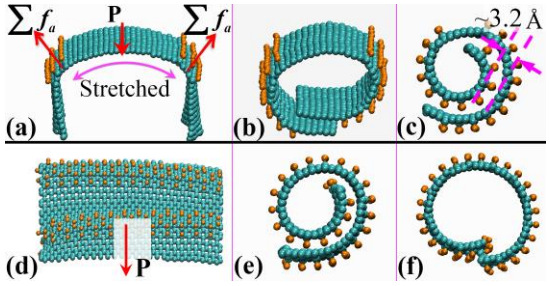

Figure 4. Morphology of the GNR (armchair-edged) with different fluorination patterns: parallel to length direction at the doping ratio of (a) 23%, (b) 54% and (c) 85%; parallel to width direction at the doping ratio of (d) 43%, (e) 71% and (f) 100%. In (a) and (d), P represents the periodic boundary condition, i.e., the length direction of GNR.

3.3 Implications

The above discussions show that the morphology of either GS or GNR can be effectively modulated through the control of C_4F fluorination pattern. An explicit implication from such interesting morphology change is the fabrication of nanoscrolls, which has been envisioned to hold appealing applications in the fields of catalysis, gas storage, and energy storage due to their large surface area.[43] Our results have shown that with the increasing width of the nanoribbon, the single-side or double-side full fluorination can perfectly drive the nanoscroll formation (roll along the length direction). Specifically, for the single-side fluorination, the deformation of the GNR (zigzag-edged) is found to transit from a single nanoscroll (Figure 4e) to symmetric coupled nanoscroll when its width is larger than ~ 8 nm, as shown in Figure 5a. The radius *r* of the inner circle is measured around 0.5 nm, with a perimeter around 3.4 nm and the interlayer distance *d* as ~4.5 Å. On the other hand, the double-side fluorination initiates the formation of anti-symmetric coupled nanoscrolls as depicted in Figure 5b. Similar phenomena have also been observed from the armchair-edged GNRs and graphene with controlled hydrogenation as reported by Reddy and Zhang.[38]

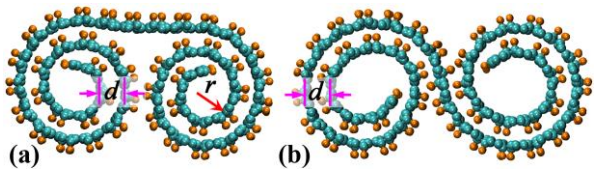

Figure 5. Formation of nanoscrolls from GNRs (width of ~19.6 nm, length of ~ 3.4 nm) with: (a) single-side C_4F fluorination; (b) double-side C_4F fluorination.

It is also relevant to assess how the fluorination will impact the morphology of multi-layer GNRs. Our results show that the out-of-plane force resulted from the double-side full C_4F fluorination can induce the interlayer sliding in a bi-layer zigzag-edged GNR (Figure 6a). Particularly, when the bi-layer GNR's width is smaller than ~ 1.7 nm, or between ~ 1.7 and ~ 5.1 nm, the two graphene layers will roll up in different directions but still adhere to each other by the interlayer van der Waals forces (Figure 6b and 6c). However, other GNRs,

the two graphene layers will not only roll up along different directions but also separate from each other as depicted in Figure 6d and 6e. Similar phenomena are also observed for the armchair-edged bi-layer GNRs. These findings suggest an interesting avenue to fabricate nanoscrolls from bi-layer GNRs.

Further testing reveals that the strong out-of-plane force could even deform a tri-layer GNR into a nanoscroll structure. As seen in Figure 6f, the pristine mid-layer of the sample has been bent and rolled up into a nanoscroll (width of ~ 6.4 nm, length of ~ 6 nm). By increasing the layer number, a climbing phenomenon of the fluorinated graphene layer due to the sliding is observed. Specifically, the climbing behavior is determined by the stacking sequence of the graphene layer. For the AB stacking model considered herein, the fluorinated layer will slide from the right to the left (lateral) direction (see Figure 6a), and induce different morphologies when the layer number changes from even to odd as compared in Figure 6g and 6h. Similarly, the single-side full C_4F fluorination in multi-layer GNRS can induce two morphology modes, including the bent structure, and the climbing phenomenon (see Supporting Information, S4).

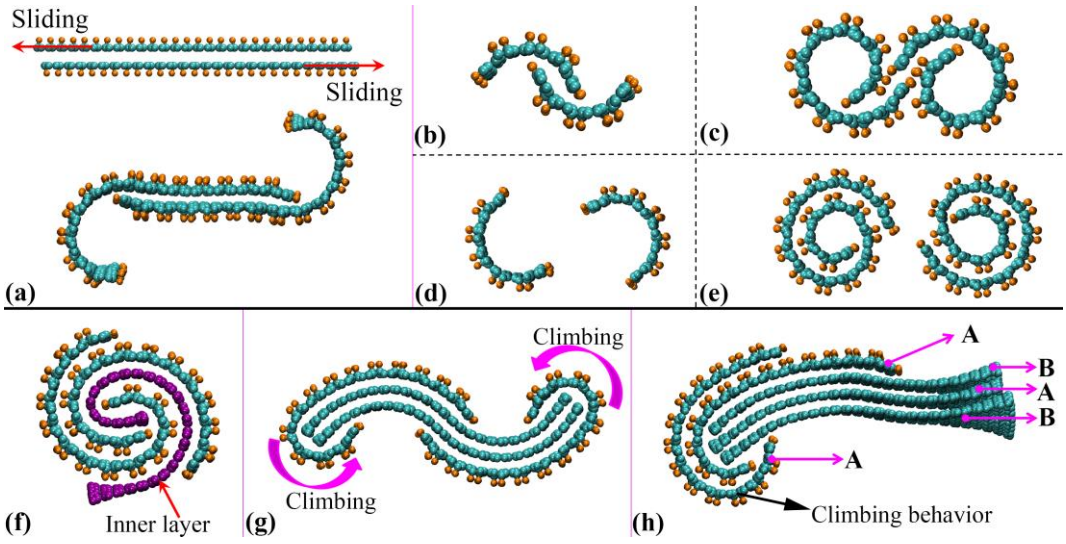

Figure 6. Morphology changes of multi-layer GNR with double-side fluorination: (a) interlayer sliding phenomenon; morphologies of fully double-side fluorinated bi-layer GNRs with a width of (b) 1.7 nm, (c) 4.3 nm, (d) 2.6 nm and (e) 5.1 nm; (f) Formation of nanoscroll

from a tri-layer GNR; The climbing phenomenon for GNRs containing (g) four layers and (h) five layers.

Before concluding, we also extend the discussion on the tensile properties of GNR with patterned fluorination. According to above discussion, we can allocate four fluorination patterns (including 128 F atoms in a total of 3968 atoms) along the length direction of the GNR (size of ~ 4 × 25.5 nm^2), which will thus change the original flat GNR into a zigzag structure (see Figure 7a). Such morphology change will shrink the GNR and thus modify its tensile behavior. As compared in Figure 7b, the tensile strain energy of the zigzag structure (the blue line) increases slowly until the structure resumes to the initial length of a pristine GNR. Afterwards, the strain energy profile appears almost overlapped with that obtained from a pristine GNR (the red line). According to the continuum mechanics, the effective Young's modulus E can be derived from the strain energy (ΔU) *vs* strain (ε) curve by following $\Delta U / V_0 = E\varepsilon^2 / 2 + \xi E\varepsilon^3 / 3$, here V_0 is the initial volume and ξ is a constant.[44] The nearly overlapped strain energy curves in Figure 7b (after the zigzag fluorinated GNR resuming to flat) indicate that the fluorination has an insignificant influence to the Young's modulus of the GNR by considering that the F atoms do not increase much of the system volume. After passing a threshold value, the strain energy experiences a sharp drop, indicating a brittle behavior of the fluorinated GNR. Taking this threshold point as the yielding point of the structure, the much smaller yielding strain energy indicates a much smaller yielding strength by following the virial stress method.[44] On the other hand, benefiting from the buckled structure, the fluorinated GNR shows an effective yielding strain about 0.33 ($\varepsilon = \Delta L / L_0$) which is about 40% larger than that of its pristine counterpart ($\varepsilon_y = 0.23$). These results suggest that the patterned fluorination can be used to tune the mechanical properties of GNR, targeting the applications for flexible or stretchable electronics.

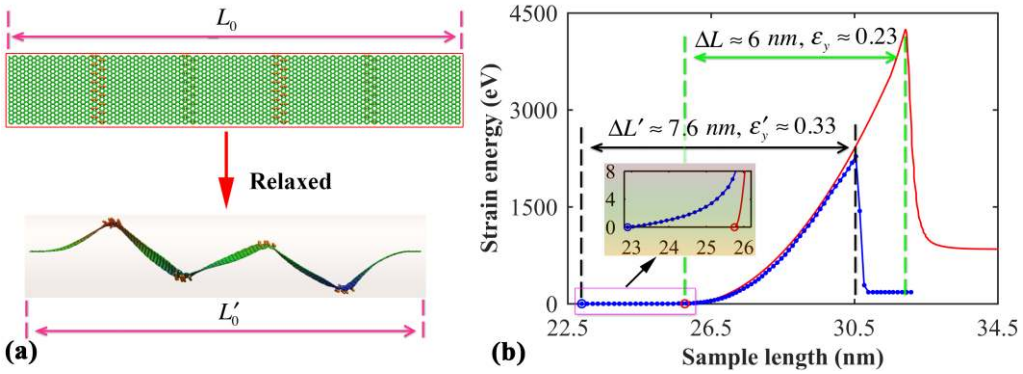

Figure 7. (a) The GNR with patterned double-side fluorination before and after energy relaxation; (b) Strain energy *vs* length curves from the pristine GNR (red line) and its counterpart with double-side fluorination (blue line), inset enlarges the strain energy curve at the sample length from 23 to 26 nm.

4. CONCLUSIONS

An extensive investigation of the impacts on the GS and GNR from patterned fluorination has been conducted based on the recently developed ReaxFF potential. The applied ReaxFF potential has been specifically optimized for the carbon-fluorine cluster systems (based on first principle calculations), which can well reproduce their key quantum mechanical and thermal properties. It is found that the morphology of either GS or GNR can be effectively modulated by controlling the C_4F fluorination pattern. Depending on the width, doping ratio, and configuration of fluorination pattern, the initial monolayer GS or GNR can deform into a zigzag, folded, ruffle, nanoscroll, and chain structures. The strong out-of-plane forces from the double-side fluorination pattern are also found to delaminate the graphene layers from a bi-layer GNR (generating two nanoscrolls), roll up a tri-layer GNR into a nanoscroll and induces climbing phenomenon for GNR with four or more layers. Further studies show that the tensile properties of GNR can be effectively controlled through fluorination pattern, e.g., the existence of fluorination pattern is found to greatly extend the elastic deformation region of the GNR. This study shows an effective avenue to tailor the morphologies and mechanical

properties of GS and GNR, which should be beneficial for their various applications, such as gas storage, energy storage, and flexible or stretchable electronics.

ACKNOWLEDGEMENT

Supports from the ARC Discovery Project (DP130102120), the Recruitment Program of Global Young Experts (China), Fundamental Research Funds for the Central Universities (DUT14RC(3)002), and the High Performance Computer resources provided by the Queensland University of Technology are gratefully acknowledged. In addition, we thank our colleague, Edmund Pickering, for proof reading.

SUPPLEMENTARY INFORMATION

Supplementary information is available for the results from the fluorinated graphene sheet with patterned C_2F-boat fluorination, the graphene sheet with double-side C_4F fluorination along zigzag direction, the armchair-edged graphene nanoribbon with double-side C_4F fluorination, the multilayer graphene nanoribbon with single-side C_4F fluorination, and a summary of all examined model details and some representative initial configurations.

REFERENCES NOTES

(1) Novoselov, K.; Fal, V.; Colombo, L.; Gellert, P.; Schwab, M.; Kim, K., A Roadmap for Graphene. *Nature* **2012,** *490*, 192-200.
(2) Pop, E.; Varshney, V.; Roy, A. K., Thermal Properties of Graphene: Fundamentals and Applications. *MRS Bull.* **2012,** *37*, 1273-1281.
(3) Neto, A. C.; Guinea, F.; Peres, N.; Novoselov, K. S.; Geim, A. K., The Electronic Properties of Graphene. *Rev. Mod. Phys.* **2009,** *81*, 109.
(4) Balandin, A. A.; Ghosh, S.; Bao, W.; Calizo, I.; Teweldebrhan, D.; Miao, F.; Lau, C. N., Superior Thermal Conductivity of Single-Layer Graphene. *Nano Lett.* **2008,** *8*, 902-907.
(5) Du, X.; Skachko, I.; Barker, A.; Andrei, E. Y., Approaching Ballistic Transport in Suspended Graphene. *Nat. Nanotechnol.* **2008,** *3*, 491-495.
(6) Peigney, A.; Laurent, C.; Flahaut, E.; Bacsa, R. R.; Rousset, A., Specific Surface Area of Carbon Nanotubes and Bundles of Carbon Nanotubes. *Carbon* **2001,** *39*, 507-514.
(7) Lee, C.; Wei, X.; Kysar, J. W.; Hone, J., Measurement of the Elastic Properties and Intrinsic Strength of Monolayer Graphene. *Science* **2008,** *321*, 385-388.
(8) Bonaccorso, F.; Colombo, L.; Yu, G.; Stoller, M.; Tozzini, V.; Ferrari, A. C.; Ruoff, R. S.; Pellegrini, V., Graphene, Related Two-Dimensional Crystals, and Hybrid Systems for Energy Conversion and Storage. *Science* **2015,** *347*, 1246501.

(9) Zhang, H.; Grüner, G.; Zhao, Y., Recent Advancements of Graphene in Biomedicine. *Journal of Materials Chemistry B* **2013,** *1*, 2542-2567.
(10) Zhang, X.; Hu, M.; Giapis, K. P.; Poulikakos, D., Schemes for and Mechanisms of Reduction in Thermal Conductivity in Nanostructured Thermoelectrics. *J. Heat Transfer* **2012,** *134*, 102402-102402.
(11) Shin, H. J.; Choi, W. M.; Choi, D.; Han, G. H.; Yoon, S. M.; Park, H. K.; Kim, S. W.; Jin, Y. W.; Lee, S. Y.; Kim, J. M., Control of Electronic Structure of Graphene by Various Dopants and Their Effects on a Nanogenerator. *J. Am. Chem. Soc.* **2010,** *132*, 15603.
(12) Lv, R.; Terrones, M., Towards New Graphene Materials: Doped Graphene Sheets and Nanoribbons. *Mater. Lett.* **2012,** *78*, 209-218.
(13) Mali, K. S.; Greenwood, J.; Adisoejoso, J.; Phillipson, R.; De Feyter, S., Nanostructuring Graphene for Controlled and Reproducible Functionalization. *Nanoscale* **2015,** *7*, 1566-1585.
(14) Deng, Z.; Smolyanitsky, A.; Li, Q.; Feng, X.-Q.; Cannara, R. J., Adhesion-Dependent Negative Friction Coefficient on Chemically Modified Graphite at the Nanoscale. *Nat. Mater.* **2012,** *11*, 1032-1037.
(15) Pei, Q.; Zhang, Y.; Shenoy, V., A Molecular Dynamics Study of the Mechanical Properties of Hydrogen Functionalized Graphene. *Carbon* **2010,** *48*, 898-904.
(16) Pei, Q. X.; Zhang, Y. W.; Shenoy, V. B., Mechanical Properties of Methyl Functionalized Graphene: A Molecular Dynamics Study. *Nanotechnology* **2010,** *21*, 115709.
(17) Yazyev, O. V.; Louie, S. G., Electronic Transport in Polycrystalline Graphene. *Nat. Mater.* **2010,** *9*, 806-809.
(18) Sha, Z.; Quek, S.; Pei, Q.; Liu, Z.; Wang, T.; Shenoy, V.; Zhang, Y., Inverse Pseudo Hall-Petch Relation in Polycrystalline Graphene. *Scientific reports* **2014,** *4*.
(19) Georgakilas, V.; Otyepka, M.; Bourlinos, A. B.; Chandra, V.; Kim, N.; Kemp, K. C.; Hobza, P.; Zboril, R.; Kim, K. S., Functionalization of Graphene: Covalent and Non-Covalent Approaches, Derivatives and Applications. *Chem. Rev.* **2012,** *112*, 6156-6214.
(20) Reddy, C.; Zhang, Y.; Shenoy, V., Patterned Graphone—a Novel Template for Molecular Packing. *Nanotechnology* **2012,** *23*, 165303.
(21) Zhao, F.-G.; Zhao, G.; Liu, X.-H.; Ge, C.-W.; Wang, J.-T.; Li, B.-L.; Wang, Q.-G.; Li, W.-S.; Chen, Q.-Y., Fluorinated Graphene: Facile Solution Preparation and Tailorable Properties by Fluorine-Content Tuning. *J. Mater. Chem. A* **2014,** *2*, 8782-8789.
(22) Karlicky, F. s.; Kumara Ramanatha Datta, K.; Otyepka, M.; Zboˇril, R., Halogenated Graphenes: Rapidly Growing Family of Graphene Derivatives. *ACS Nano* **2013,** *7*, 6434-6464.
(23) Wang, Z.; Wang, J.; Li, Z.; Gong, P.; Liu, X.; Zhang, L.; Ren, J.; Wang, H.; Yang, S., Synthesis of Fluorinated Graphene with Tunable Degree of Fluorination. *Carbon* **2012,** *50*, 5403-5410.
(24) Nair, R. R.; Ren, W.; Jalil, R.; Riaz, I.; Kravets, V. G.; Britnell, L.; Blake, P.; Schedin, F.; Mayorov, A. S.; Yuan, S., et al., Fluorographene: A Two-Dimensional Counterpart of Teflon. *Small* **2010,** *6*, 2877-2884.
(25) Şahin, H.; Topsakal, M.; Ciraci, S., Structures of Fluorinated Graphene and Their Signatures. *Phys. Rev. B* **2011,** *83*, 115432.
(26) Liu, H. Y.; Hou, Z. F.; Hu, C. H.; Yang, Y.; Zhu, Z. Z., Electronic and Magnetic Properties of Fluorinated Graphene with Different Coverage of Fluorine. *J. Phys. Chem. C* **2012,** *116*, 18193-18201.
(27) Robinson, J. T.; Burgess, J. S.; Junkermeier, C. E.; Badescu, S. C.; Reinecke, T. L.; Perkins, F. K.; Zalalutdniov, M. K.; Baldwin, J. W.; Culbertson, J. C.; Sheehan, P. E., et al., Properties of Fluorinated Graphene Films. *Nano Lett.* **2010,** *10*, 3001-3005.
(28) Withers, F.; Bointon, T. H.; Dubois, M.; Russo, S.; Craciun, M. F., Nanopatterning of Fluorinated Graphene by Electron Beam Irradiation. *Nano Lett.* **2011,** *11*, 3912-3916.
(29) Lee, W.-K.; Haydell, M.; Robinson, J. T.; Laracuente, A. R.; Cimpoiasu, E.; King, W. P.; Sheehan, P. E., Nanoscale Reduction of Graphene Fluoride Via Thermochemical Nanolithography. *ACS Nano* **2013,** *7*, 6219-6224.
(30) Avouris, P., Graphene: Electronic and Photonic Properties and Devices. *Nano Lett.* **2010,** *10*, 4285.

(31) Singh, S. K.; Srinivasan, S. G.; Neek-Amal, M.; Costamagna, S.; van Duin, A. C.; Peeters, F., Thermal Properties of Fluorinated Graphene. *Phys. Rev. B* **2013,** *87*, 104114.
(32) Van Duin, A. C.; Dasgupta, S.; Lorant, F.; Goddard, W. A., Reaxff: A Reactive Force Field for Hydrocarbons. *J. Phys. Chem. A* **2001,** *105*, 9396-9409.
(33) Hoover, W. G., Canonical Dynamics: Equilibrium Phase-Space Distributions. *Phys. Rev. A* **1985,** *31*, 1695-1697.
(34) Nosé, S., A Unified Formulation of the Constant Temperature Molecular Dynamics Methods. *J. Chem. Phys.* **1984,** *81*, 511.
(35) Plimpton, S., Fast Parallel Algorithms for Short-Range Molecular Dynamics. *J. Comput. Phys.* **1995,** *117*, 1-19.
(36) Zhang, L.; Zeng, X.; Wang, X., Programmable Hydrogenation of Graphene for Novel Nanocages. *Scientific reports* **2013,** *3*.
(37) Kashtiban, R. J.; Dyson, M. A.; Nair, R. R.; Zan, R.; Wong, S. L.; Ramasse, Q.; Geim, A. K.; Bangert, U.; Sloan, J., Atomically Resolved Imaging of Highly Ordered Alternating Fluorinated Graphene. *Nat Commun* **2014,** *5*.
(38) Reddy, C.; Zhang, Y.-W., Structure Manipulation of Graphene by Hydrogenation. *Carbon* **2014,** *69*, 86-91.
(39) Kudin, K. N.; Scuseria, G. E.; Yakobson, B. I., C_2f, Bn, and C Nanoshell Elasticity from Ab Initio Computations. *Phys. Rev. B* **2001,** *64*, 235406.
(40) Li, Q.; Liu, X.-Z.; Kim, S.-P.; Shenoy, V. B.; Sheehan, P. E.; Robinson, J. T.; Carpick, R. W., Fluorination of Graphene Enhances Friction Due to Increased Corrugation. *Nano Lett.* **2014,** *14*, 5212-5217.
(41) Wang, X., Graphene Nanoribbons: Chemical Stitching. *Nat Nano* **2014,** *9*, 875-876.
(42) Shenoy, V.; Reddy, C.; Ramasubramaniam, A.; Zhang, Y., Edge-Stress-Induced Warping of Graphene Sheets and Nanoribbons. *Phys. Rev. Lett.* **2008,** *101*, 245501.
(43) Mpourmpakis, G.; Tylianakis, E.; Froudakis, G. E., Carbon Nanoscrolls: A Promising Material for Hydrogen Storage. *Nano Lett.* **2007,** *7*, 1893-1897.
(44) Diao, J.; Gall, K.; Dunn, M. L., Atomistic Simulation of the Structure and Elastic Properties of Gold Nanowires. *J. Mech. Phys. Solids* **2004,** *52*, 1935-1962.

Table of Contents

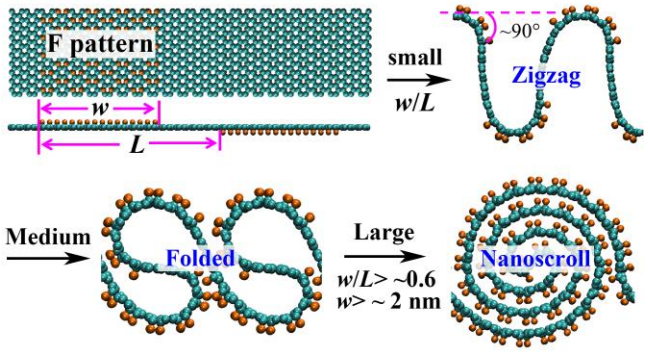

Morphology change of graphene with patterned fluorination.